Stiffness transitions in Si_xSe_{1-x} glasses from Raman scattering and temperature-modulated differential scanning calorimetry

D. Selvanathan, W. J. Bresser, and P. Boolchand
Department of ECECS, University of Cincinnati, Cincinnati, Ohio 45221-0030
(Received 23 September 1998; revised manuscript received 9 April 1999)

Temperature-modulated differential scanning calorimetry (MDSC) measurements on Si_xSe_{1-x} glasses show glass transitions to be *thermally reversing* in character in the composition window $0.20<x<0.27$. Raman scattering shows a trimodal distribution of vibrational modes, identified with corner-sharing (CS), edge-sharing (ES), and Se-chain modes (CM). In the floppy region, $0<x<0.19$, these modes are symmetric and are characteristic of a *random network*. In the transition region, $0.20<x<0.27$, the ES and CM split into doublets suggesting appearance of extended range structural correlations. In the percolatively rigid region, $x>0.27$, the CS mode in addition to the ES and CM also splits into a doublet indicating growth of substantial medium range structure. The large compositional width ($0.20<x<0.27$) associated with Raman elastic thresholds coincides with the thermally reversing window from MDSC.

I. INTRODUCTION

The nature of the floppy to rigid transition in network glasses continues to be one of the central issues in glass science that could impact other areas of condensed-matter science. Unlike many other transitions encountered in physics which occur either as a function of temperature or pressure or an external field, the stiffness transition manifests most directly in the elastic behavior of a network as a function of connectivity or mean coordination number ($\overline{r}$). Changes in network connectivity of glasses in the laboratory are achieved by compositional tuning a binary or a ternary glass system. Compositional changes lead inevitably to changes in glass molecular structure. Understandably therefore the stiffness transition has structure-related consequences, noted[1] in microscopic measurements nearly a decade back. The physics of the transition itself has stimulated broad interest. It is widely believed that the glass forming tendency of melts are optimized in the vicinity of the stiffness transition. It may provide a means to understand the origin of glass forming tendency in inorganic glasses, in organic polymers and in biological macromolecules where different types of forces come into play and serve as mechanical constraints[2] to freeze in disorder as melts are cooled.

Historically, ideas on the stiffness transition evolved in 1979 from attempts to develop a microscopic theory[2] of glass formation, and application of percolation theory[3] to describe onset of rigidity. J. C. Phillips suggested that for a covalently bonded network constrained by bond-stretching (α) and bond-bending (β) forces, the glass forming tendency will be optimized when the number of constraints/atom (n_c) equal the degrees of freedom (n_d). Enumeration of α and β constraints for a three-dimensional (3D) network showed that the condition

$$n_c = n_d \tag{1}$$

is satisfied when the mean-coordination number ($\overline{r}$) of a network acquires a critical value 2.40:

$$\overline{r} = \overline{r}_c = 2.40. \tag{2}$$

M. F. Thorpe[3] recognized that a normal mode analysis of undercoordinated networks ($\overline{r}<\overline{r}_c$) yields zero-frequency or floppy mode solutions, whose number per atom f equals

$$f = n_d - n_c. \tag{3}$$

In a mean-field theory, the variation of f with network connectivity $\overline{r}$ is linear, and rigidity onsets when f extrapolates to zero as $\overline{r}$ increases to 2.40. Subsequently, more realistic model variations of $f(\overline{r})$ emerged from numerical simulations on atypical (diamond) networks and showed $f(\overline{r})$ to decrease linearly with $\overline{r}$ at $r<2.40$ and to vary exponentially at $\overline{r}>2.40$. More recently, numerical simulations on 2D generic networks containing a million atoms or more have become feasible using an integer algorithm.[4] For 3D networks, such simulations on atypical networks reveal that the stiffness transition occurs close to the mean-field value at $\overline{r}_c = 2.385$. A variety of experiments on inorganic glasses have revealed[5,6] anomalies near a mean coordination of 2.40. Of these experiments elastic constants[7,8] and low-frequency vibrational density of states measurements[9,10] have been particularly insightful in elucidating aspects of the stiffness transition. The existence of a solitary stiffness transition in glasses near $\overline{r}=2.40$, however, has become a matter of some recent discussions. J. C. Phillips has recently suggested[11] that effective medium theories of disordered solids are likely to be poor approximations near phase transitions, and that there may actually be two stiffness transitions. In the face of these interesting ideas, it becomes essential to establish those generic features of experimental results that are model independent to understand the nature of the stiffness transition in glasses.

The binary Si_xSe_{1-x} glass system represents an attractive prototypical IV-VI glass system in which mean-field theory would predict the stiffness transition to occur near the glass composition $x\sim0.20$ corresponding to $\overline{r}_c=2.40$. The fourfold coordination of Si and twofold coordination of Se in these glasses has been verified by neutron diffraction[12] and

Se *k*-edge x-ray fine-structure measurement.[12] The glass system has been the subject of Raman scattering[13–16] and IR absorption,[17] Si^{29} solid-state nuclear magnetic resonance[18] (NMR), in addition to differential scanning calorimetry[19] (DSC) and Molar volume measurements[17] as well. The molecular structure of these glasses at $x \leqslant \frac{1}{3}$ has been modeled both in terms of a stochastic random network,[16] and in terms of a cross-linked edge-sharing (ES)-chain network.[14] Given the wealth of these structure results, the Si_xSe_{1-x} binary glass system appears to be particularly attractive for the proposed stiffness transition studies. Our interest in this binary also stems from the fact that we have recently examined[6] the onset of rigidity in a companion IV-VI glass system, the Ge_xSe_{1-x} binary. It is of interest to compare and contrast results on these two binaries and to establish features of elasticity and glass structure that are common as well as different, results that are likely to have a bearing on the physical nature of the stiffness transition in glasses.

Our present Raman-scattering studies complemented by temperature modulated differential scanning calorimetry measurements reveal that there are two stiffness transitions in the Si_xSe_{1-x} binary glass system; transition 1 at $x = x_c(1) = 0.20(1)$ corresponding to a mean coordination of 2.40, and transition 2 at $x = x_c(2) = 0.270(5)$ corresponding to a $\overline{r} = 2.54(1)$. Transition 1 represents the onset while transition 2 the completion of rigidity in a percolative sense. Furthermore, the optical elastic measurements show that transition 1 appears second order while transition 2 first order in nature. The consequences of these observations in relation to the stiffness transition in chalcogenide glasses are discussed.

The paper is organized in five sections as follows. Details of sample synthesis and characterization by Raman scattering and modulated differential scanning calorimetry (MDSC) appear in Sec. II. Raman line-shape deconvolution procedures used and the ensuing vibrational spectroscopy results are presented in Sec. III. The implications of the vibrational spectroscopy results on glass molecular structure, and the nature of the stiffness transition in the Si-Se binary are discussed in Sec. IV. The principal conclusions of this work are summarized in Sec. V.

II. EXPERIMENT

A. Sample synthesis and handling

99.9999% Si chips and 99.9999% Se chips from Cerac, Inc. were weighed in the desired proportion and reacted in evacuated (5×10^{-7} Torr) quartz tubings at 1100 °C for typically 5–7 days with intermittent mixing. Melt size was kept at 2 g at each composition. Quartz tubings of 5-mm i.d. and a 6-mm o.d. were baked at 900 °C and pumped down to 5×10^{-7} Torr prior to vacuum encapsulation of the starting materials. Melt temperatures were then lowered to $T_l + 50$ °C and the melts equilibrated for several hours at the lower temperature prior to a quench in cold water. Here T_l represents the liquidus temperature, and values of T_l were taken from the known phase diagram[14,19] of the Si-Se binary.

Si_xSe_{1-x} glasses are known to be moisture prone and give out a rather unpleasant odor due to formation of H_2Se in a humid ambient. For this reason, the micro-Raman measurements on the glass samples were performed in the quartz tubings used to synthesize the samples. For scanning calorimetric measurements, glass samples were transferred to hermetically sealed Al pans, in a glove box using dry N_2 gas as an ambient. For MDSC measurements, Al pans and lids were thoroughly dried by heating in a vacuum line, prior to hermetically sealing the samples in a dry nitrogen ambient using a glove box.

The three polymorphs of *c*-$SiSe_2$ were synthesized as follows. The high-temperature (ht) phase was obtained by cooling homogeneous $SiSe_2$ melts to 800 °C and retaining them at that temperature for a week. A different process was employed to obtain the metastable medium-temperature (mt) and low-temperature (lt) phases. The starting elemental chips in the desired ratio were thoroughly crushed to a fine powder, first separately and then mixed together in the desired ratio. The mixtures were sealed in evacuated quartz ampules after several purges with He gas. The mt phase was obtained by slowly (10 °C/h) bringing the mixture up to 525 °C and retaining it at that temperature for several weeks. The lt phase was obtained by a parallel heating process, except the final temperature of the mixture was held at 400 °C for a week. Reaction of the elements to produce the desired polymorph could be monitored *in situ* by periodically recording Raman spectra of the samples in the quartz tubings. The lt phase and the stoichiometric glass appeared reddish-brown, while the mt and the ht phase yellowish-orange in color.

B. Glass transitions and nonreversing heat flow

Glass transition temperatures T_g were established using a Model 2920 temperature modulated differential scanning calorimeter (MDSC) from TA Instruments, Inc. In contrast to a DSC, in an MDSC scan, one programs a sinusoidal temperature variation superposed on the linear T ramp. This permits deconvoluting the total endothermic heat flow near the glass transition into a reversing and a nonreversing component.[20] The reversing component tracks the sinusoidal T variation, and is ascribed to thermodynamic specific heat changes in a sample upon heating. On the other hand, the nonreversing heat flow component is ascribed to kinetic processes and the enthalpic changes accompanying structural reorganization of the glass network as it softens near T_g.

Typical MDSC scan rate conditions used were as follows. The linear temperature ramp was programmed to have a slope of 3 °C per 60 sec, while the sinusoidal temperature variation to have an amplitude of 1 °C and a time period of 100 sec. Figures 1–3 provide examples of MDSC scans of present glasses; Fig. 1 represents an MDSC trace taken at low x ($x = 0.15$), Fig. 2 at medium x ($x = 0.22$), and Fig. 3 at high x ($x = 0.333$). At each composition, we established T_g and ΔC_p from the reversing heat flow using the inflection point of the endotherm to define the T_g. Thus, even though a glass transition is typically 30 °C wide, the inflection point can reproducibly localize the transition to less than 2 °C. Note that the shape of the total heat-flow endotherm changes with glass composition due to the kinetic heat-flow component. On the other hand, the reversing heat-flow component of the endotherm always displayed a characteristic steplike change at T_g. At all glass compositions the nonreversing heat-flow peak occurs as a *precursor* to the softening transition (T_g) as can be seen in the Figs. 1–3 (compare nonre-

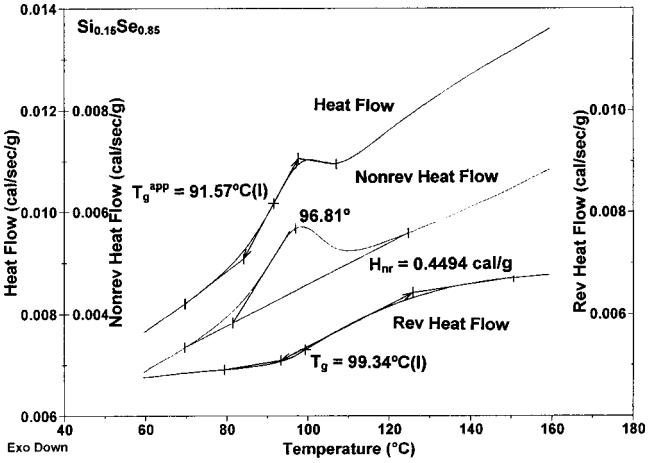

FIG. 1. MDSC scan of a $Si_{0.15}Se_{0.85}$ glass showing the heat flow (total), deconvoluted into the nonreversing and the reversing heat flow. The presence of a sizeable nonreversing heat flow in this undercoordinated glass shifts the apparent glass transition T_g^{app} (accessible from the heat flow) to a lower value by 8 °C in relation to the T_g deduced from the reversing heat flow. Excursions along positive y axis represent endothermic processes.

versing heat-flow and reversing heat-flow scans). Figure 4(a) provides a summary of $T_g(x)$ variation in the present binary glasses. One finds that the $T_g(x)$ variation is monotonically increasing with x and the slope dT_g/dx increases remarkably at $x>0.31$. We also note that T_g at $x=0.34$ is larger than at $x=\frac{1}{3}$ with the slope dT_g/dx decreasing sharply once $x>\frac{1}{3}$. The smooth $T_g(x)$ variation of Fig. 4(a) has also proved to be a useful check of glass compositions in synthesis of samples.

The MDSC scans of Figs. 1–3 also reveal a sizable nonreversible heat flow (ΔH_{nr}) in glasses at low x (undercoordinated) and at high x (overcoordinated), with a minimum in ΔH_{nr} occurring in the mid-x region (near optimal coordination). In Fig. 4(b), we have plotted the nonreversing heat-flow $\Delta H_{nr}(x)$ variation, and find that it displays a broad and nearly flat minimum that begins sharply near $x_c(1)=0.20$ and ends abruptly near $x_c(2)=0.27$. The intrinsic value of

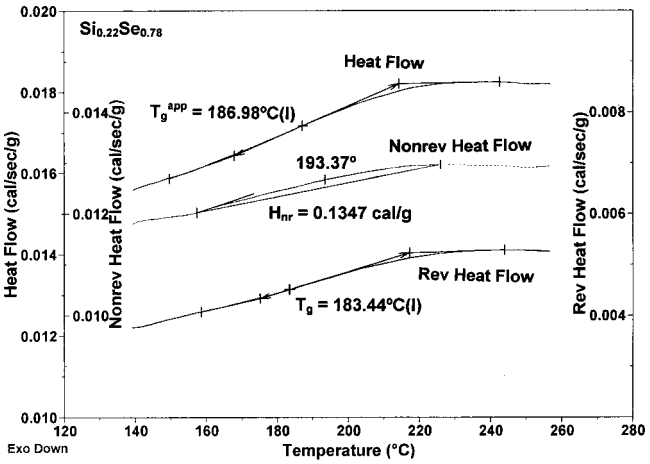

FIG. 2. MDSC scan of a $Si_{0.22}Se_{0.78}$ glass showing T_g^{app} and T_g approach each other as the nonreversing heat-flow endotherm (ΔH_{nr}) decreases qualitatively when the network becomes optimally coordinated.

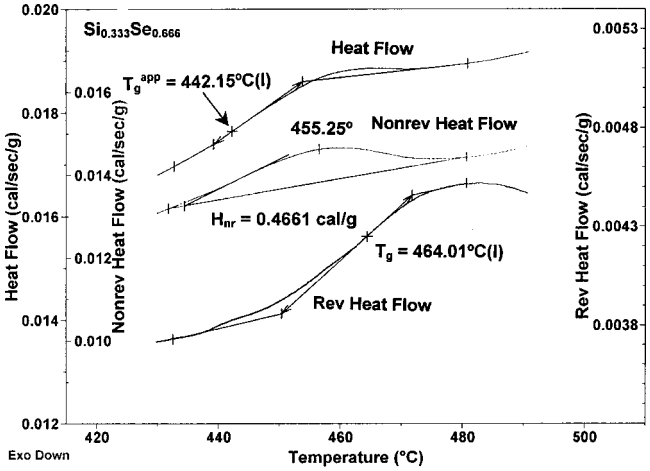

FIG. 3. MDSC scan of a $SiSe_2$ glass displaying a sizeable ΔH_{nr} in an overcoordinated glass which results in T_g^{app} being nearly 22 °C less than T_g. See Fig. 1 caption and text for details.

MDSC in glass science studies derives from the ΔH_{nr} term that appears to be correlated to the stiffness transition as we shall discuss later.

The glass transitions deduced from the total heat-flow scans will henceforth be labeled as T_g^{app} and these afford a means to compare the present MDSC results with previous

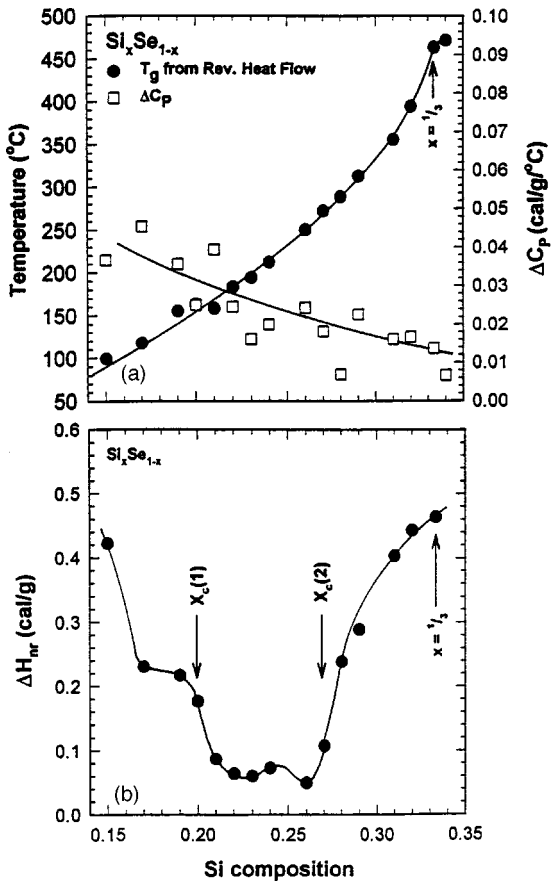

FIG. 4. (a) $T_g(x)$ and $\Delta C_p(x)$ variation and (b) $\Delta H_{nr}(x)$ as a function of Si concentration x in binary Si_xSe_{1-x} glasses. Note that $T_g(x)$ and $\Delta C_p(x)$ vary monotonically with x, while $\Delta H_{nr}(x)$ displays a threshold behavior, a broad and deep minimum in the $0.21<x<0.26$ composition range.

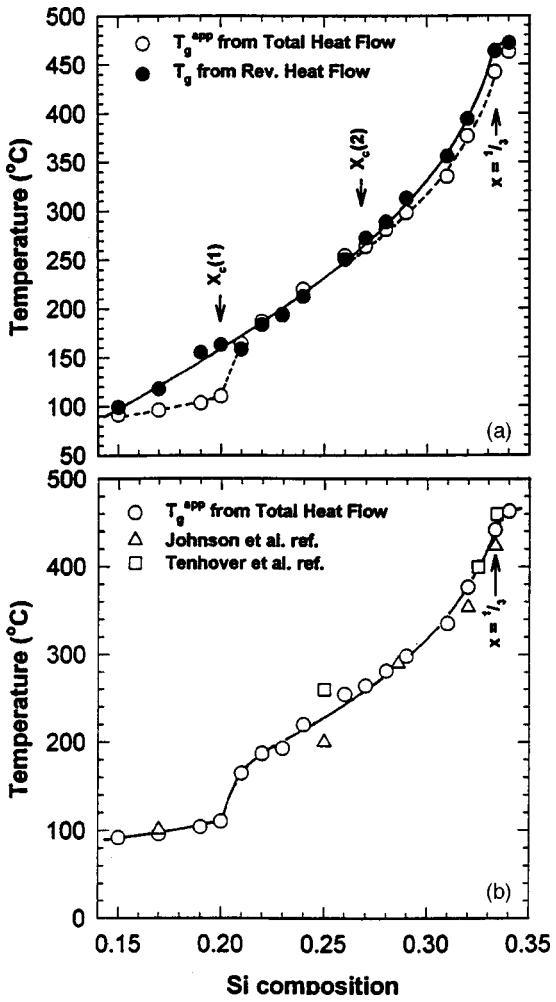

FIG. 5. (a) $T_g^{app}(x)$ and $T_g(x)$ variation in Si_xSe_{1-x} glasses deduced from MDSC measurements revealing $T_g^{app}(x) < T_g(x)$ when nonreversing heat-flow processes occur in undercoordinated $[x < x_c(1)]$ and overcoordinated $[x > x_c(2)]$ glasses. (b) $T_g^{app}(x)$ correlates well with previous T_g results from DSC measurements of Johnson *et al.* (Ref. 12) and M. Tenhover *et al.* (Ref. 17) at indicated Si_xSe_{1-x} glass compositions.

DSC results on these glasses. Our T_g^{app} variation [Fig. 5(b)] is in good agreement with the work of Tenhover *et al.*[17] and Johnson *et al.*[19] The presence of kinetic heat-flow processes can cause apparent shifts in the T_g^{app} from the actual T_g. This is more clearly seen in Fig. 5(a), where we compare the T_g^{app} and T_g on Si_xSe_{1-x} glasses from our MDSC measurements. The sudden jump in T_g^{app} when x increases to 0.20 can be traced to $\Delta H_{nr} \rightarrow 0$. Likewise, the deviation between T_g and T_g^{app} at $x > x_c(2)$ grows [Fig. 5(a)] as ΔH_{nr} increases [Fig. 4(b)], but it is much smaller than the jump near $x_c(1)$. The kinetic heat flow is also related to sample history. For example, a second MDSC scan at $x = 0.15$ taken immediately following one on a virgin glass (that has relaxed at room temperature for days), reveals a significantly smaller nonreversing heat flow, understandably because relaxation processes in such undercoordinated glasses are slow, as discussed elsewhere.[20] For these reasons, MDSC measurements were taken on virgin glass samples that had relaxed at room temperature for weeks.

C. Raman-scattering procedure

Spectra of the glasses were taken with a Model T64000 triple monochrometer system from Instruments S.A. equipped with a charge-coupled device (CCD) detector and a microscope attachment. The magnification of the microscope objective was 80X yielding a spatial resolution of 1–2 μm. The 647.1-nm line from a Kr^+ ion laser was used to excite the scattering, and light was detected in a back scattering configuration. In our experiments, we used 1.25 mW of laser power on a glass sample (encapsulated in a quartz tube) to excite the scattering. At this low power level, the glass sample temperature was established to be 27 ± 5 °C from the Raman Stokes-anti-Stokes scattering intensity ratio.[21] When we increased the laser power level to 2.25 mW, the sample temperature increased to 67 ± 5 °C. Larger signals could be obtained from the glass samples at the higher laser power but we also noticed subtle changes in the observed Raman line shapes of the glasses, suggesting possibly, the presence of photostructural effects. For these reasons, Raman-scattering measurements were performed consistently at 1.25 mW of incident laser power at all glass compositions.

The triple monochrometer system was calibrated using a Ne discharge lamp which revealed three atomic transitions at 84.38, 146.38, and 299.63 cm^{-1} in the CCD spectral window (10–390 cm^{-1}). The window was kept unchanged throughout the measurements. In fact, the stability of the spectrometer system was tracked periodically by recording Ne spectra during the course of the Raman measurements. The entrance slit width was kept at 50 μm (0.78 cm^{-1}) for recording the Ne calibration lines and at 200 μm (3.12 cm^{-1}) for recording spectra of the glasses. Spectra of the glasses were averaged over nine accumulations, each lasting 9 sec. A minimum of three locations on a glass sample were studied. Each spectrum was least-squares fit to a superposition of appropriate number of Gaussians to extract mode-centroid ($\overline{\nu}$) mode width (Γ) and mode-normalized scattering strength (A), using a software package called Labcalc marketed by Galactic, Inc. We were unable to detect spatial variations in the Raman line shapes of our glass samples that would suggest presence of inhomogeneities due to incomplete alloying.

D. Compositional dependence of Raman spectra

Figure 6 provides representative spectra of the glasses taken at low x, medium x, and high x, respectively. Starting at $x = 0.15$, spectra of the glasses broadly consist of three modes, centered approximately at 210, 225, and at 260 cm^{-1}, which have been identified previously[13–16] and will henceforth be labeled as CS (corner sharing), ES (edge sharing), and CM (chain mode), respectively. We generally observed the scattering strengths of the CS and ES modes to increase at the expense of the CM as the Si content x of the glasses increased in the $0.15 < x < 0.333$ range. Furthermore, at $x \geqslant 0.19$, the ES mode, the CS mode, and CM each displayed increasingly asymmetric line shapes which could be deconvoluted into doublets as will be discussed in detail later. Splitting of the ES mode from a broad unimodal band into a doublet becomes conspicuous at compositions $x > 0.265$. We also noted that the scattering strengths of the high-frequency component of the ES mode, the bond bending mode at 70 cm^{-1}, and the bond-stretching doublet feature at 350 cm^{-1},

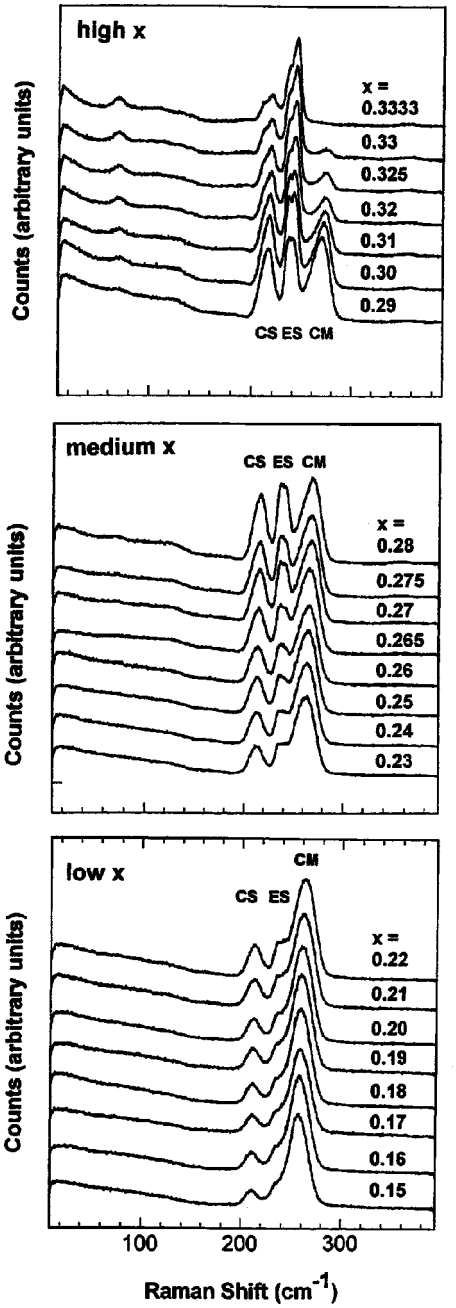

FIG. 6. Raman scattering in Si_xSe_{1-x} glasses revealing growth in scattering strength of the $Si(Se_{1/2})_4$ CS and ES modes at the expense of Se CM with x. Note that modes are symmetric at low x (lowest panel) become asymmetric at medium x (middle panel) and split at high x (top panel).

each progressively grows as x increases to $\frac{1}{3}$. These modes will be shown to be signatures of a specific cluster which we shall return to discuss in Sec. IV.

E. Raman spectra of stoichiometric $SiSe_2$ glass and crystals

The structure of only one of the crystalline polymorphs, the high-temperature (ht) phase of $SiSe_2$ has been analyzed.[22] It is indexed on an orthorhombic cell in the D_{2h}^{26} space group and consists of infinitely long parallel chains of edge-sharing $Si(Se_{1/2})_4$ tetrahedra running parallel to the crystallographic c axis. Recently, two other polymorphs, a mt and a lt phase,

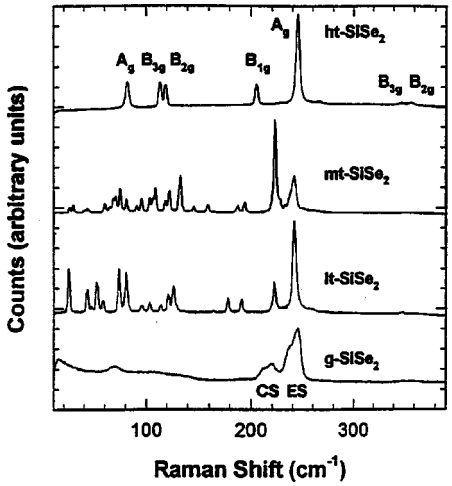

FIG. 7. Raman scattering in the ht, mt and lt polymorphs of c-$SiSe_2$ compared to that in $SiSe_2$ glass. Note that all polymorphs show mode of ES tetrahedra near 245 cm^{-1}. Mode of CS tetrahedra are observed in the mt and lt crystalline phases and the stoichiometric glass.

have been synthesized.[23] The Raman and Si^{29} NMR of the three $SiSe_2$ polymorphs have been reported.[24] The crystallographic structure of the mt and lt phases has yet to be solved, to the best of our knowledge. The Raman-scattering and NMR results on the mt and lt polymorphs reveal unequivocally presence of CS, in addition to ES, tetrahedra.

We confirm the existence of the mt and lt phase of c-$SiSe_2$. In Fig. 7 we compare Raman spectra of the three polymorphs of crystalline $SiSe_2$ with the stoichiometric g-$SiSe_2$. These results are generally in agreement with the earlier report of A. Pradel *et al.*[24] The comparison unequivocally shows that the high-frequency member of the ES mode in the glass almost coincides in frequency with the A_g mode of the ht-crystalline polymorph[14] at 245.58 cm^{-1} but deviates somewhat from the ES mode either in the mt (239.86 cm^{-1}) or the lt phase (241.97 cm^{-1}) of c-$SiSe_2$. Furthermore, the A_g mode at 80 cm^{-1} in the ht crystal has an analog at 70 cm^{-1} in the glass. The weakly excited B_{2g} and B_{3g} phonons at 345 and 355 cm^{-1} in the ht crystal[14] also have doublet counterparts centered at 350 cm^{-1} in the glass spectrum. On the other hand, the CS-mode feature in the glass has counterparts in the lt and mt $SiSe_2$ polymorph.[24] In particular, the ES to CS mode scattering strength ratio in the lt phase and the stoichiometric glass appear superficially similar. The presence of a large number of lattice modes (100 cm^{-1} and below) in the lt and mt phases is akin to those encountered in 2D form of $GeSe_2$, and these results are suggestive of crystal structures possessing large unit cells. It is likely that in these $SiSe_2$ crystalline polymorphs, chains of CS tetrahedra occur which are laterally coupled by dimeric ES units as in 2D form of $GeSe_2$. In Ref. 21 we provide a comparison of the present Raman results with the ^{29}Si NMR results[24] on $SiSe_2$ glass and the crystalline polymorphs of $SiSe_2$. We shall return to discuss the implications of these results on the structure of the stoichiometric glass in Sec. IV.

For completeness it would be appropriate to mention that in glasses at $x > \frac{1}{3}$, a different mode is observed at 200 cm^{-1}. This mode is not observed in either the stoichiometric glass

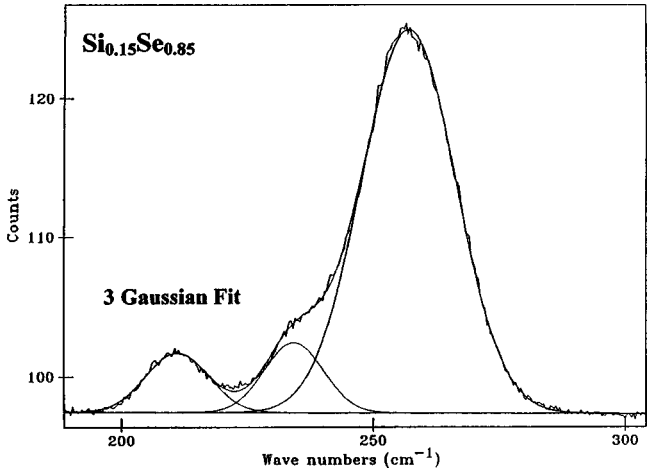

FIG. 8. Raman-scattering line shape in indicated glass deconvoluted in terms of three Gaussians reveals an excellent fit.

or the crystal at $x=\frac{1}{3}$. This mode has been attributed[14] to the appearance of face-sharing $Si_2(Se_{1/2})_6$ tetrahedra in the Si-rich glasses ($x>\frac{1}{3}$) and will henceforth not be discussed further.

III. DECONVOLUTION OF RAMAN LINE SHAPES IN GLASSES

A. Region I: Composition region $0.15<x<0.19$

In the low Si concentration range, Raman line shapes in the glasses can be well reproduced as a superposition of three symmetric Gaussians. In least-squares fitting the line shapes, we kept the mean frequency ($\overline{\nu}$), full width at half maximum (Γ), and intensity (I) of a mode as variable parameters. Such profiles are suggestive of cross linking of quasi-one-dimensional Se_n chains by Si atoms, to form *isolated* corner sharing and bi-tetrahedral edge-sharing units in a *random fashion*. Figure 8 provides an example of a line-shape deconvolution at a glass composition at $x=0.15$. Fits of a similar quality are realized up to a Si concentration of $x=0.18$.

B. Region II ($0.19<x<0.22$)

At higher Si concentrations, a deconvolution of the spectra in terms of three Gaussians appears to become inadequate. This is illustrated in Fig. 9 which shows a deconvolution of the line shape for a glass at $x=0.22$, in terms of three (top panel) as well as five Gaussians (bottom panel), with no restrictions on the line-shape parameters ($\overline{\nu},\Gamma,I$) for each of the Gaussians. The misfits on the peaks of the ES and CM, and the high-frequency shoulder of the CM is transparent in the three-Gaussian fit. These misfits can be almost eliminated by adding two more Gaussians to the fit; a companion to the ES and a companion to the CM. In a five-Gaussian fit, we found that the least-squares refinement places the companions on the high-frequency side of the majority mode. None of the line-shape parameters were kept fixed in the least-squares refinement.

The five-Gaussian deconvolution is sufficient to account for the observed line shape in the $0.19<x<0.22$ compositional range. The principal justification for the choice of five Gaussians in the fit is that the unrestricted fit parameters lead

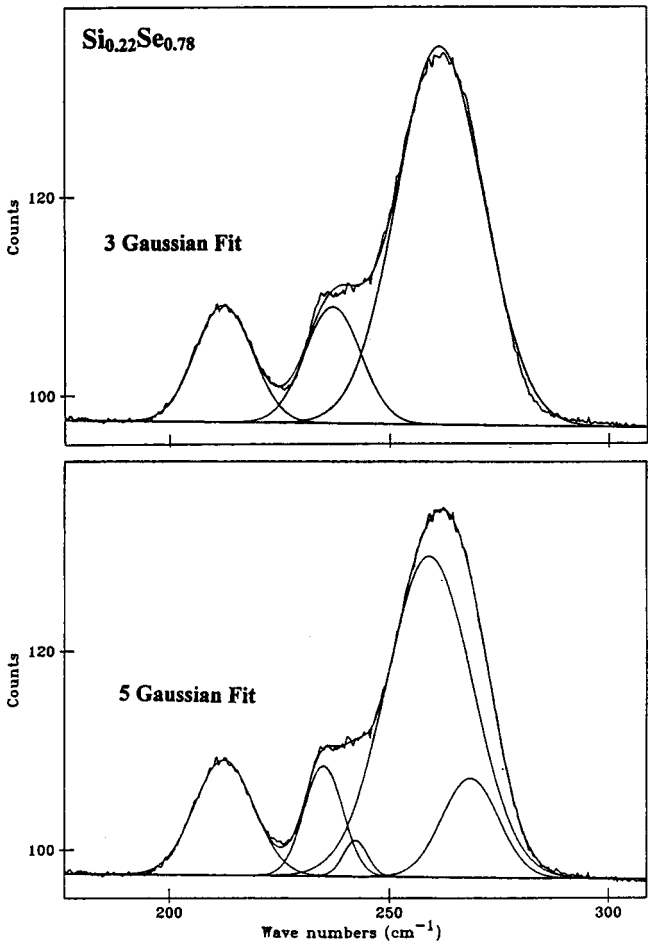

FIG. 9. Raman-scattering line shape in a $Si_{0.22}Se_{0.78}$ glass deconvoluted in terms of three (top panel) and five (bottom panel) Gaussians with no restrictions on line-shape parameters. Note that the misfits on the central- and high-frequency modes present in the three Gaussian fit are removed in the five Gaussian fit.

to the same quality of fits as measured by χ^2, and appear to change systematically with composition x as we shall discuss in Sec. III D. In this compositional range, the splitting of the ES and CM into a low-frequency and high-frequency component smoothly extrapolates to the result at low x and at high x.

In region II, spectra of the glasses suggest a transition from a random network at the low end ($x=0.19$) to a network in which structural correlations begin to appear on a scale of two or three tetrahedra at the high end ($x=0.22$). As we shall see later in Sec. IV the first of two stiffness transitions (transition 1) marking the onset of rigidity occurs near $x=0.20$.

C. Region III ($0.23<x<0.333$)

At higher Si concentrations a five-Gaussian fit to the observed line shape can be improved upon by requiring an additional Gaussian for the CS mode as the line shape becomes increasingly asymmetric. Figure 10 shows Raman spectrum of a glass at $x=0.25$ which is analyzed in terms of three and six Gaussians. Figure 11 shows a Raman spectrum of a glass at $x=0.30$, analyzed in terms of three and six Gaussians. In region III, each of the modes clearly requires

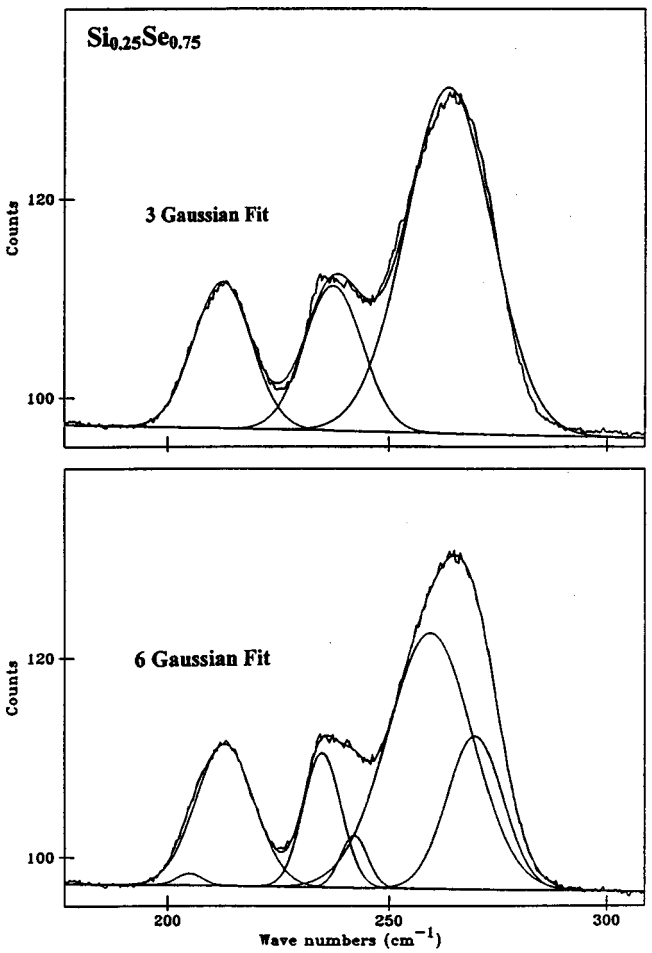

FIG. 10. Raman-scattering line shape in a $Si_{0.25}Se_{0.75}$ glass deconvoluted in terms of three (top panel) and six (bottom panel) Gaussians with no restrictions on line-shape parameters. The least-squares refinement places the companions of the CM and ES modes on the high-frequency shoulder but the companion of the CS mode on the low-frequency shoulder of the majority modes.

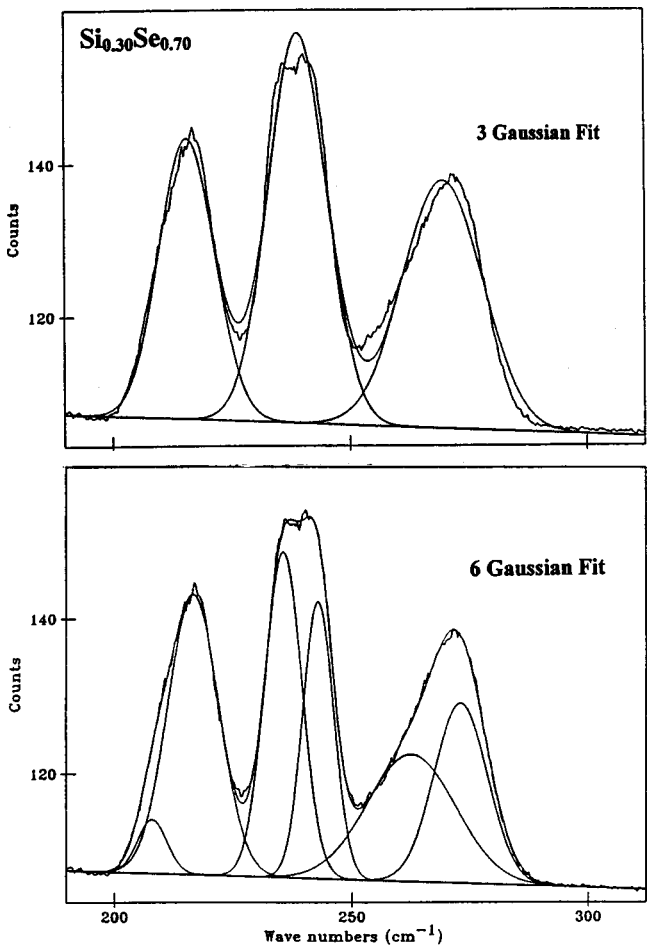

FIG. 11. Raman-scattering line shape in a $Si_{0.30}Se_{0.70}$ glass deconvoluted in terms of three (top panel) and six (bottom panel) Gaussians, with no restrictions on line-shape parameters. Note the growth in scattering strength and splitting of the ES and CS modes.

doublets. In region III the CM companion (minority mode) is placed by the refinement on the low-frequency shoulder of the main mode (majority). This is in contrast to the ES and CS modes, where the companions are placed by the refinement on the high-frequency shoulder of the majority mode.

IV. DISCUSSION

A. Raman-scattering results and mode assignments

We have identified the rationale for the fitting procedure (Secs. III A–C) used to deconvolute Raman line shapes in the three compositional regions. In this section we shall now summarize the results of this analysis and discuss mode assignments. At each composition, we have analyzed at least three sets of spectra to look for consistency before averaging the results. The result of this analysis is summarized in Figs. 13–15 which provide global compositional trends in mode parameters, and suggest specific mode assignments which will serve as a basis to discuss glass structure in Sec. IV B.

The normalized scattering strength ratios A_n/A of the CS ($n=1$), ES ($n=2$), and CM ($n=3$) as a function of x in the examined range $0.15<x<0.33$ appear in Fig. 12. As expected the CM scattering strength A_3/A extrapolates to zero as x increases to $\frac{1}{3}$. In making the plot of Fig. 14, the majority and minority mode strengths for each of the modes were added together. A particularly noteworthy feature of this plot includes a *discontinuous* change in the A_n/A ratio for the CM and ES at the composition $x=0.265$ in the middle of region III. At $x\simeq 0.27$, the increase in scattering strength of ES chain is precipitous and derives largely from a decrease in scattering strength of CM. Also noteworthy is the fact that no discontinuities manifest at the boundaries between the regions that could be an artifact of data reduction.

1. Majority and minority CS modes

The plots of Fig. 13 provide the x dependence of line-shape parameters related to the CS mode and include the mode frequency $\nu_{cs}(x)$ [Fig. 13(a)] the normalized scattering strength A_{cs}/A [Fig. 13(b)] and the linewidth $\Gamma(x)$ [Fig. 13(c)]. In region III, the CS mode splits into a majority and minority mode, with the low-frequency component (CS^{low}) representing the minority mode and the high-frequency component (CS^{high}) the majority mode. These compositional trends suggest that the majority mode in region I represents Si atoms cross-linking chains of Se_n while the minority mode

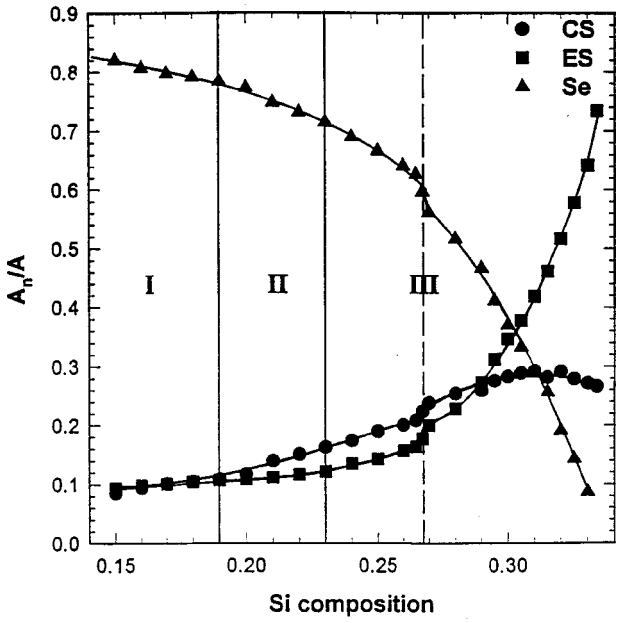

FIG. 12. Mode scattering strength $A_n/A(x)$ of the CS (●), ES (■), and CM (▲) as a function of x showing a precipitous growth of ES tetrahedra at the expense of Se_n chains $x \geqslant 0.27$.

largely represents CS Si-atoms cross-linking chains of ES units. Note that the minority mode has a narrower linewidth (~ 7 cm^{-1}) than that of the majority CS mode (14 cm^{-1}). The larger linewidth of the majority CS mode is in harmony with the floppy character of undercoordinated Se_n chains that the CS unit serves to cross link. Furthermore, the population of the minority CS mode increases with x only at $x > 0.26$ [see Fig. 13(b)] supporting the proposed assignment that the mode is related to the appearance of ES chains in the network (Fig. 12). It is, of course, unreasonable to imagine that in region III the proposed majority CS mode assignment of region I continues to be signature of Si-tetrahedra cross-linking Se_n chains, when the concentration of the latter species (Fig. 12) decreases dramatically. In regions II and III, and particularly at $x > 0.27$, the character of this mode undergoes a change, and we suggest that it then represent chains of CS tetrahedra in the network. The reduction in mode linewidth [Fig. 13(c)] and concomitant growth in the scattering strength of the majority CS mode are in harmony with such an assignment. A summary of mode assignments appears in Table I.

2. Majority and minority ES modes

The plots of Fig. 14 provide x dependence of line-shape parameters related to the ES modes. Mode frequencies of the majority and minority ES mode appear in Fig. 14(a), their normalized scattering strength ratios in Fig. 14(b), while their linewidths appear in Fig. 14(c). Perhaps the most significant feature of these compositional trends is the mode frequency variation [Fig. 16(a)] which reveals that the minority ES mode (ES^{high}) acquires a frequency of 245.3 cm^{-1} as $x \to \frac{1}{3}$. This mode frequency almost *coincides* with the A_g mode frequency in the ht $SiSe_2$ phase (Fig. 7). These results suggest that $SiSe_2$ glass consists, at least partially, of fragments of the out-of-phase (OOP) ES chains as present in the ht phase of c-$SiSe_2$. Near $x \to \frac{1}{3}$, the majority ES mode with

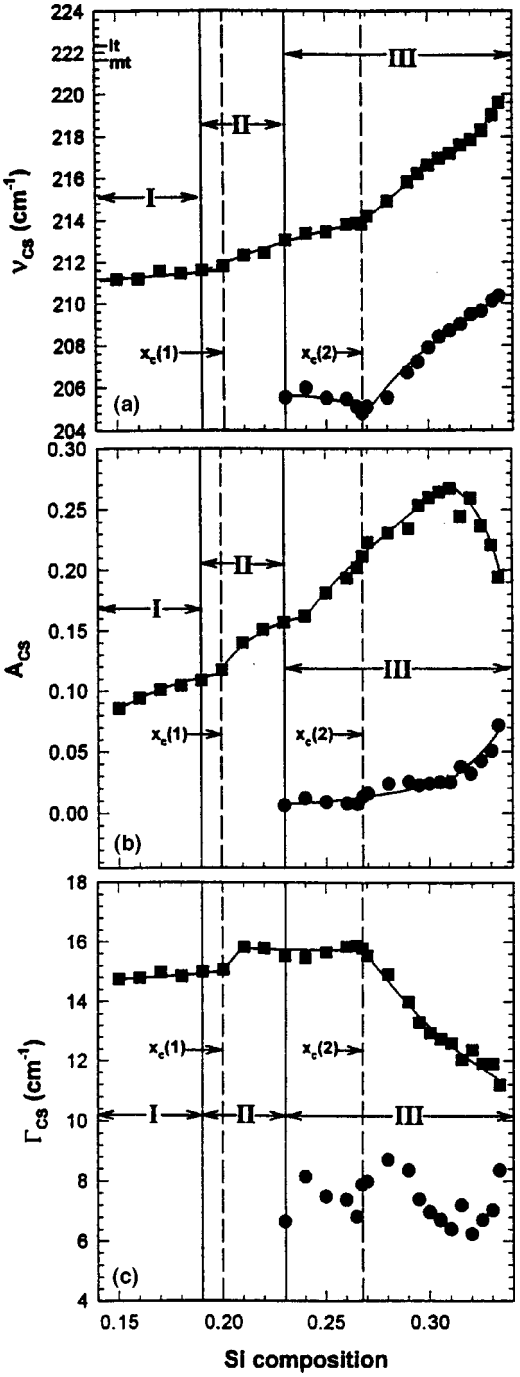

FIG. 13. Raman line-shape parameters associated with the CS mode: top panel $\nu(x)$, middle panel $A_1(x)/A$, and bottom panel $\Gamma(x)$. The CS mode splits into a majority and minority mode in region III. Continuous lines demarcate the three regions while the broken lines indicate the threshold $x_c(1)$ and $x_c(2)$ Si compositions. The error bars on mode frequencies are ± 0.1 cm^{-1} and represent the size of the data points.

a mode frequency somewhat lower than the minority ES mode frequency, is thought to result from Si tetrahedra present in ES chains that are more distant from each other than the OOP chains, such as the in-phase (IP) ES chains. Such ES chains form elements of the cross-linked chain clusters originally proposed by J. Griffiths *et al.*[14] Gladden and Elliott[25] found such a cluster to contribute at least partially to the structure factor of a glass at $x = 0.32$ in their computer

TABLE I. Summary of Raman mode assignments in Si_xSe_{1-x} glasses at $0<x<\frac{1}{3}$ suggested from present and previous reports.

Mode	Mean frequency	Low x (region I)	medium and high x (regions II and III)
ES^{high}[a]	245 cm^{-1}		at $x\rightarrow\frac{1}{3}$, mode frequency coincides with that of A_g mode of c-$SiSe_2$; A_g mode of ''out-of-phase'' ES chains (OOP chains) forming elements of CLCC
ES^{low}	236 cm^{-1}	bi-tetrahedral ES units cross linking Se_n chains	peculiar to glass; A_g mode of ''in-phase'' ES chains (IP chains) as elements of CLCR
CS^{high}	214 cm^{-1}	A_1 mode of CS tetrahedra formed as cross links of Se_n chains	chains of CS units forming part of CLCR
CS^{low}[a]	206 cm^{-1}		Minority mode; appears at $x<0.25$; mode of CS units formed as cross links of ES chains
CM^{high}[a]	270 cm^{-1}		Minority mode; appears at $x>0.19$; Se-Se stretch mode of Se pairs and/or 3-Se chain segments present at cross links of ES chains
CM^{low}	258 cm^{-1}	Se_n chain mode $n>3$, A_1 mode of disordered chains	scattering strength diminishes drastically as $x\rightarrow\frac{1}{3}$

[a]Unbold modes are minority modes.

modeling studies. Note that linewidths of the majority ES mode are in general larger than linewidths of the minority ES mode. The OOP chains (minority ES mode) are more compactly assembled motifs than IP chains (majority ES mode), and the narrower width of the former chains is a reflection of their more uniquely defined packing geometry. The geometry of the IP chains is less restrictive, and such chain fragments cross linked by chains of CS tetrahedra are likely to form elements of medium range order of the glasses at $x>0.27$, and of the lt and mt phase of c-$SiSe_2$ as suggested[24] by the ^{29}Si NMR results on these crystalline polymorphs.

At low x ($0.15<x<0.19$) and medium x ($0.19<x<0.23$), the majority ES mode frequencies are significantly lower (by 3 cm^{-1}) than their values near $x\rightarrow\frac{1}{3}$ [Fig. 14(a)]. At low x, the majority mode probably represents a mode of isolated bi-tetrahedral ES units, i.e., $Si_2(Se_{1/2})_6$ units, serving to cross link Se_n chain segments. At medium x, these bi-tetrahedral ES units become cross linked by CS units, nucleating a cross-linked chain-ring (CLCR) structure. This view is corroborated with the near halving of the majority mode linewidth [shown in Fig. 14(c)] with x in the $0.15<x<0.30$ range. One expects mode widths of isolated ES units in Se_n chains to be larger because of the intrinsic floppiness of the chains. Formation of CLCR leads to a more connected structure, and the narrower mode widths are a consequence of the underlying ring structure. The ES chains comprising the CLCR structure grow in concentration with x, and this results in a packing problem, reflected in an increase in mode width and molar volumes[19] as $x>0.30$.

3. Majority and minority chain modes

The plots of Fig. 15 provide the x dependence of lineshape parameters of CM. For the CM, we had noted that the majority mode frequency (CM^{high}) is, in general, higher than the minority mode (CM^{low}) frequency. The normalized scattering strength ratios of the majority and minority CM appear in Fig. 15(b), and as expected both strengths extrapolate to nearly zero as $x\rightarrow\frac{1}{3}$ when the chains are fully cross linked. We also find that the linewidth of the majority CM is, in general, larger than the minority CM linewidth [Fig. 15(c)]. The mode frequencies, mode linewidths, and mode-scattering strengths for the majority CM in the present glasses have analogies in Ge_xSe_{1-x} glasses, and these results are persuasive to suggest that the majority CM represents an A_1 symmetric stretch mode of disordered Se chains. The minority CM manifests at $x>0.20$, and we tentatively identify it with Se dimers and possibly Se trimers present at the cross links of ES chains with CS units. In the proposed models of the cross-linked chain-cluster (CLCC) and CLCR, Se atoms serve to bridge between CS and ES units. It is likely that for the more distant and therefore loosely packed IP chains, Se dimers and/or trimers instead of Se atoms serve to bridge ES and CS units. Such short Se chain segments may help provide strain relief as bridges. Such chain segments are identified with the minority CM in the spectra of the Si_xSe_{1-x} glasses.

We have summarized in Table I, the mode assignments suggested by the compositional trends in Raman mode frequencies, widths, and scattering strengths in the present glass system. The underlying eigenvectors are briefly commented upon in the remainder of this subsection.

The A_1 mode of CS mode involves a symmetric stretch of the four nearest-neighbor Se atoms along the tetrahedral bond directions with the central Si cation remaining stationary.[14,16] For an isolated CS unit, the mode in question involves only the Si-Se bond-stretching force constant and it largely determines the frequency of the mode to be about 210 cm^{-1}. Such a mode in a network glass of CS tetrahedra is not expected to be entirely localized on a tetrahedra because of intertetrahedral couplings. The Se bridging angles are close to but not exactly 90°. Thus presence of intertetrahedral couplings will delocalize the mode, broaden it, and also increase the mode frequency with increasing connectivity of the network. In fact, the success of Raman scattering as a probe of local elasticity in a network glass crucially rests on the presence of these intertetrahedral couplings.

In contrast to the eigenvectors of the Raman active A_1 mode of CS units, those of the A_g mode of ES units involve

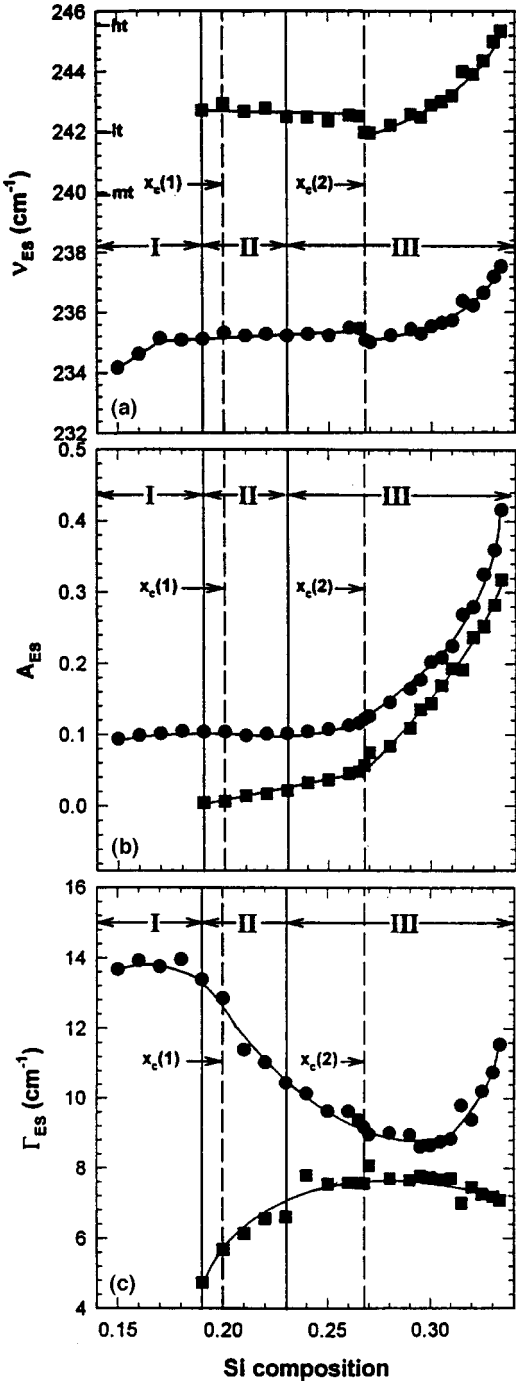

FIG. 14. Raman line-shape parameters associated with the ES mode: top panel $\nu(x)$, middle panel $A_2(x)/A$, and bottom panel $\Gamma(x)$. The ES mode splits into a majority and minority mode in regions II and III. See text for details. The error bars on mode frequencies are ± 0.1 cm^{-1} and represent the size of the data points.

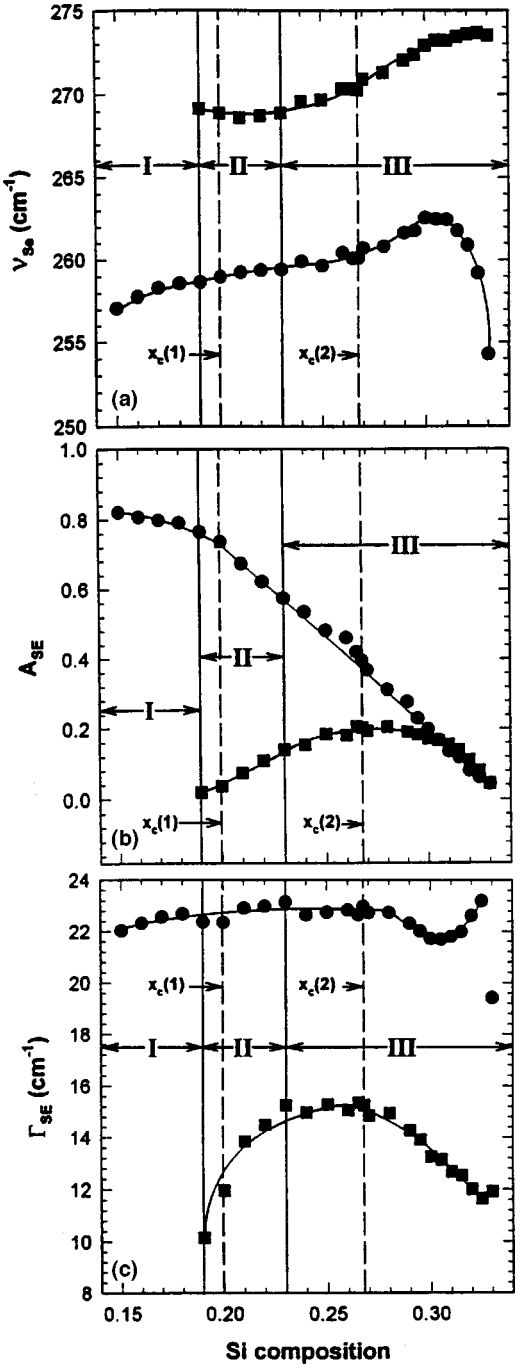

FIG. 15. Raman line-shape parameters of Se chain mode (CM), showing top panel $\nu(x)$, middle panel $A_3(x)/A$, and bottom panel $\Gamma(x)$. The chain mode splits into a majority and minority mode in regions II and III. The error bars on mode frequencies are ± 0.1 cm^{-1} and represent the size of the data points.

displacements[14,16] of the Se atoms at right angles to the two-fold axis of a tetrahedral unit (or the axis of ES units) and is therefore not a pure bond-stretching mode.

The A_1 mode of helical chains of Se as in trigonal Se is a symmetric breathing mode in which Se atoms displace normal to the chain axis.[27] In a glass, chains are distorted and the A_1 mode, although broadened, continues to have the same microscopic origin. The A_1 mode in a Se glass (250 cm^{-1}) is significantly upshifted in relation to that in *t*-Se (236 cm^{-1}) and, at least one view[20,27] attributes the shift to the more isolated or molecular character of chains present in a glass in relation to those in the crystal.

B. Glass molecular structure evolution with connectivity

The richness of the Raman scattering line shapes in the glasses, and particularly their variation with changes in glass composition as small as $\Delta x = 0.01$, as seen presently, provides crucial insights on the evolving molecular structure. Glass structure in the chalcogenides has had its share of con-

troversies, and the present binary is no exception. A stochastic random networks model description of these glasses was developed by Sugai[16] to account for the Raman spectra across the whole composition range $0<x<\frac{1}{3}$. On the other hand, a specific molecular fragment consisting of chains of ES $Si(Se_{1/2})_2$ tetrahedra cross linked by CS ones was proposed by J. Griffiths *et al.*[14] to account for the observed Raman modes in the glasses. The latter model has also found support in attempts to develop computer models of an $x=0.32$ glass, to account for the observed elastic neutron structure factor. These structure factor results[26] also found little support for a stochastic random network at $x=0.32$.

In region I, it appears that chains and rings of Se are cross linked by Si atoms in a random fashion by isolated CS units and by isolated bi-tetratedral ES units [Fig. 16(a)]. Indeed, deconvolution of Raman line shapes in terms of three symmetric Gaussians is a very good representation of the data and suggests that a stochastic random network description of these glasses at $x\leqslant 0.19$ is a reasonable description.[16]

With increasing x, and particularly in regions II and III, line-shape deconvolution in terms of three Gaussians becomes rather inadequate, suggesting appearance of extended range structures, such as the CLCR and CLCC structures emerge as illustrated in Figs. 16(b) and 16(c). In the rings (CLCR) in-phase ES chains are cross linked by chains of CS units while in the cluster (CLCC), out-of-phase ES chains are cross linked by CS units. The majority (minority) CS mode represent signature of CLCR (CLCC) medium range structures as illustrated in Table I. The majority (minority) ES modes likewise also provide signature of CLCR (CLCC) structures.

In region III, perhaps the most striking feature of the Raman results is the discontinuous jump at $x=0.27$ followed by a precipitous growth ($x>0.27$) in scattering strength of ES tetrahedra at the expense of Se chain modes (with relatively little change in scattering strength of CS tetrahedra). In this composition range evidence for growth in concentration of CLCC structures occurs. In the Raman spectrum, one observes growth in scattering strength of both the 70- and 240-cm^{-1} modes (counterpart of the Ag modes of ht $SiSe_2$) along with the 345 and 350-cm^{-1} doublet (counterpart of B_{2g} and B_{3g} modes of ht $SiSe_2$). In fact, the frequency of the minority ES mode in $SiSe_2$ glass actually coincides with that of the A_g mode frequency in the ht-$SiSe_2$ phase. These results taken together constitute evidence for CLCC structure of the out-of-phase ES chains as found in the ht phase of c-$SiSe_2$ populated in the stoichiometric glass.

There are, however, other vibrational features of $SiSe_2$ glass that resemble those of the mt and lt phase of $SiSe_2$ consisting of CLCR structures. For example, in both these crystalline polymorphs modes of CS tetrahedra occur with varying concentration ratios of ES to CS tetrahedra. In this respect, the ^{29}Si NMR results on the $SiSe_2$ polymorphs are far more quantitative, and reveal directly the concentrations of Si tetrahedra having zero, $E(0)$; one, $E(1)$; or two $E(2)$; edge-sharing nearest neighbors as illustrated in Figs. 16(a)–(c). Thus only $E(2)$ signatures appear in the ht $SiSe_2$ as one would expect based on the infinitely long ES chains present in the known crystal structure. In the mt and lt polymorphs, observed ratios of $E(2):E(1):E(0)$ equal 2:2:1 and 1:1:0, respectively, which may be contrasted to ratios of 1:2:1 in the stoichiometric glass. One possible interpretation of these results is that the mt-crystalline phase consists largely of CLCR's, while the lt-crystalline phase consists of CLCC structures, a speculation that could be checked by solving the crystal structures of these phases. The structure of the stoichiometric glass thus has features of not only the ht- but also the lt- and mt-crystalline phases.

The optical band gap $E_g(x)$ variation with x in the present glasses reveals a sharp increase[17] from 2.30 to 3.35 eV as x increases in the narrow composition range 0.325–0.340, and the color of the glasses changes from a gray-black ($x\leqslant 0.32$) to orange (0.33) to yellow (0.34). In the same composition interval glass transition temperatures $T_g(x)$ increase at a higher rate [Fig. 4(a)]. A first-principles theoretical attempt to understand T_g changes with network connectivity for random networks has now been made by Kerner and Micoulaut.[28] Clearly, changes in optical and thermal properties accompany evolution of substantial medium range structure in these glasses, providing perhaps one of the more striking changes in structure with composition ever documented in a chalcogenide.

Given the richness of the present Raman results, it would be of interest to carry forward a program of molecular-dynamic simulations[30] and to supplement in a more quantitative fashion the present molecular structure description of Si_xSe_{1-x} glasses. Such studies should also provide important insights into the molecular origin of the onset of rigidity in steps.

C. Stiffness transitions in Si_xSe_{1-x} glasses

The CS-, ES-, and CM-mode frequency variation with glass composition, $\nu_{cs}(x)$, $\nu_{es}(x)$, and $\nu_{se}(x)$ plotted in Figs. 13(a), 14(a), and 15(a) are reproduced in Fig. 17 to facilitate a comparison. In this section we shall analyze these variations and show that the observed trends provide evidence for two stiffness transitions, an onset point at $x=x_c(1)$ labeled transition 1 and a completion point at $x=x_c(2)$ labeled transition 2.

ES units forming part of a chain are overcoordinated ($\overline{r}=2.67$) and comprise the rigid regions of the network. Se_n-chain fragments possessing $\overline{r}=2$, on the other hand, comprise the floppy regions of the network. CS units play a dual role; such units when cross-link Se_n-chain fragments probe the dynamics of these floppy chains, on the other hand when CS units form part of a chain of CS tetrahedra or cross-link ES chains these probe the dynamics of these rigid fragments. For these reasons, the mode frequency variation of ES and CM, provide directly the optical elastic response of the rigid and floppy regions in Si_xSe_{1-x} glasses. On the other hand, mode frequency variation of CS tetrahedra displays a richer structure because of the dual role displayed by such units probing both the rigid and the floppy regions.

There are several general features that become transparent from the global trends shown in Fig. 17. The elastic response (mode frequency squared) of the CM remains always sublinear in x across the connectivity range investigated. On the other hand, the elastic response of ES tetrahedra which is independent of x at $x<x_c(2)$, displays a superlinear response at $x>x_c(2)$, unambiguously identifying the composition $x_c(2)$ above which the network has become percola-

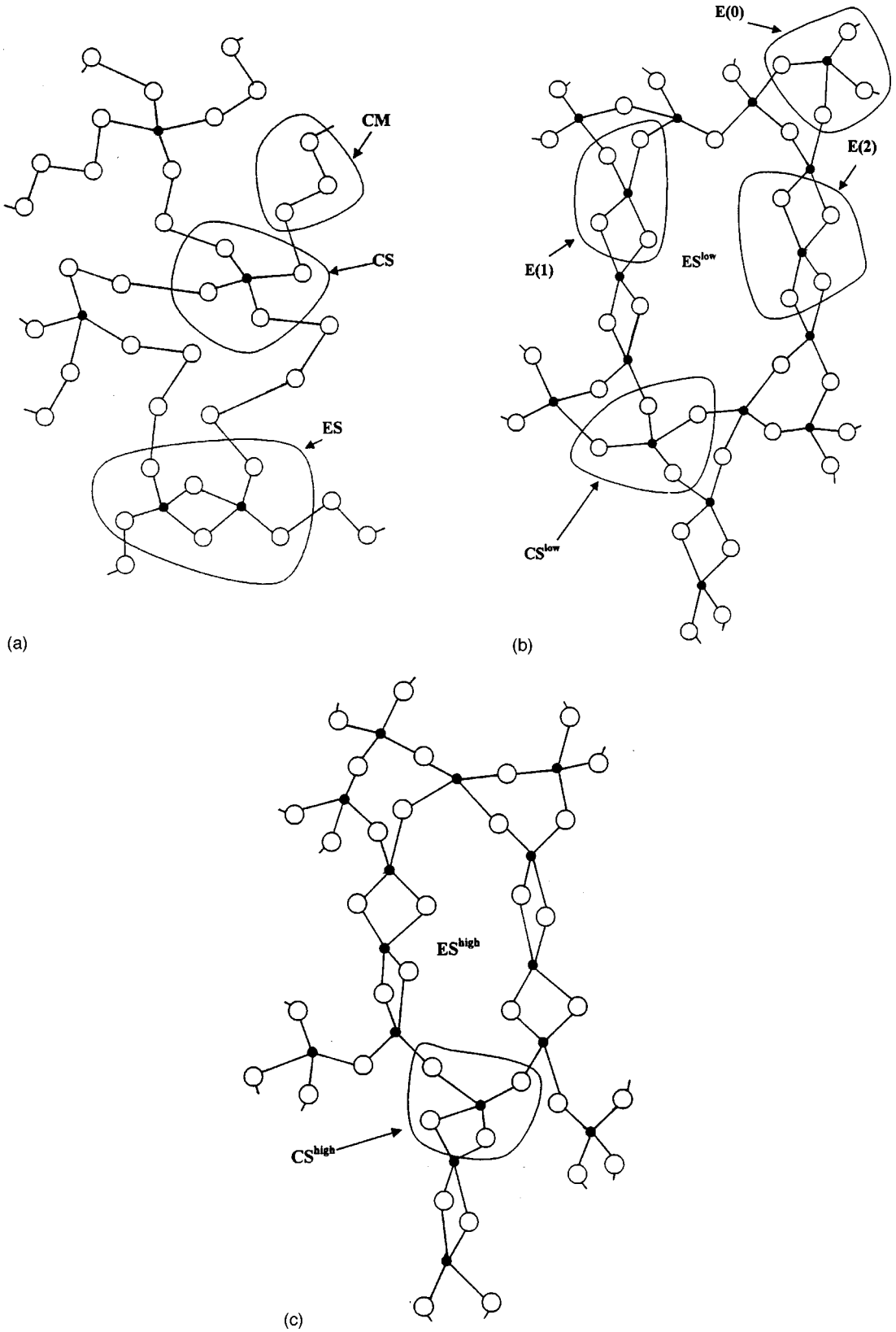

FIG. 16. Molecular structure of Si_xSe_{1-x} glasses suggested by Raman-scattering measurements. The ball and stick models illustrate aspects of short- and medium-range structures at (a) low x, (b) medium x, showing a CLCR structure, and (c) high x, showing a CLCC structure. See Table I for additional details.

tively rigid. But perhaps the most revealing elastic response comes from the CS units that reveal distinct kinks (change in slope) at $x=x_c(1)$ and $=x_c(2)$. We observe a sublinear variation in the optical elasticity in the transition region $x_c(1)<x<x_c(2)$, but a superlinear one thereafter, at $x>x_c(2)$. It is transparent that Si_xSe_{1-x} glasses are rigid in a percolative sense only at $x>x_c(2)$ and are floppy at $x<x_c(1)$, with a rather wide transition region $[x_c(1)<x$

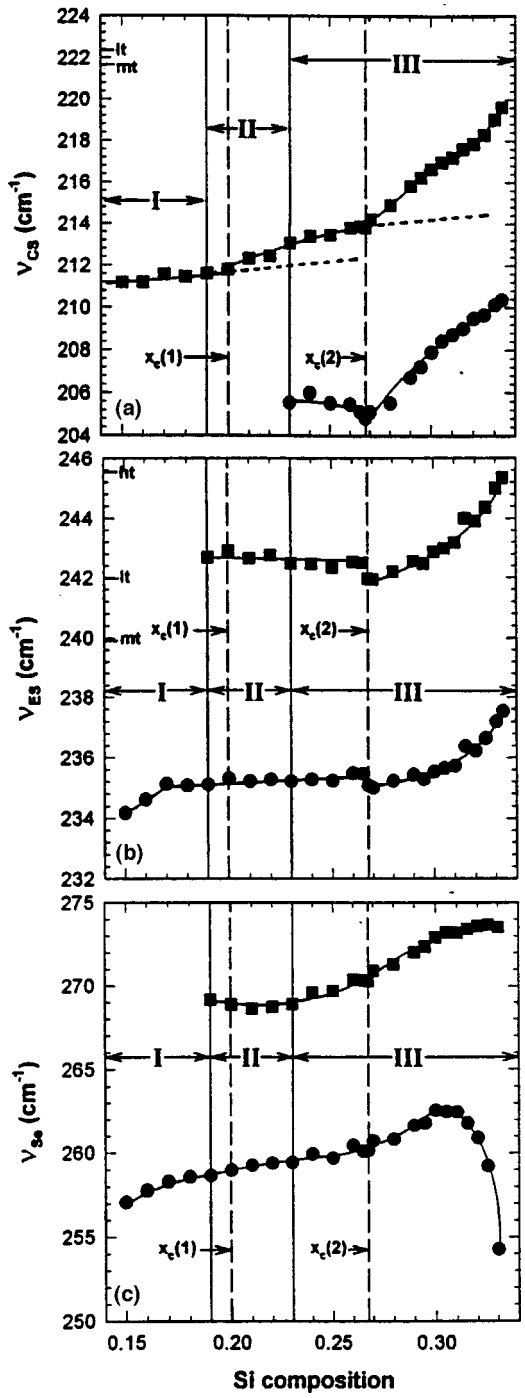

FIG. 17. Raman mode frequency variation of CS tetrahedra (top panel), ES tetrahedra (middle panel), and CM (bottom panel) as a function of x in Si_xSe_{1-x} glasses. See text for details. The error bars on mode frequencies are ± 0.1 cm^{-1} and represent the size of the data points.

$<x_c(2)]$ over which a mechanical stiffening of the network occurs.

1. Floppy region

Glass compositions at $x<0.20$ are considered to be generally floppy since Se_n-chain fragments comprise the majority phase at low Si concentrations. In region I, $\nu_{cs}(x)$ varies linearly with x, and one observes a *mild* slope $d\nu_{cs}(x)/dx = 0.12\,\mathrm{cm}^{-1}$ at. %Si. It would be instructive to recall here

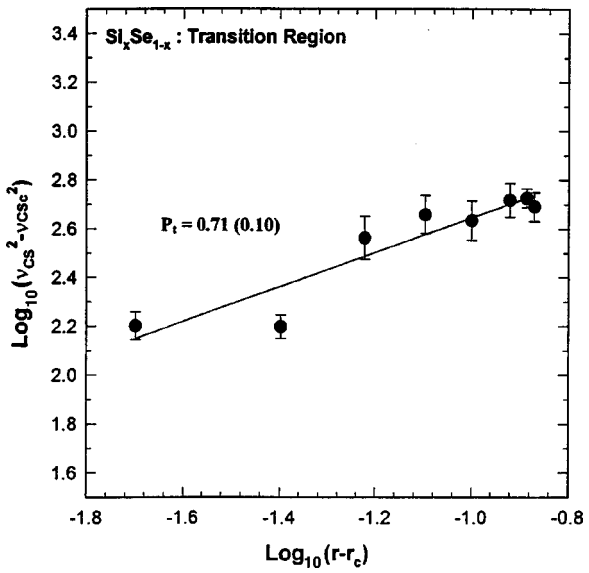

FIG. 18. Local elasticity in the transition region $x_c(1) \leqslant x \leqslant x_c(2)$ is well described by a sublinear power law of $p_t = 0.71(10)$.

that numerical simulations[31,32] of elastic response of a bond-depleted diamond lattice reveal a flat response or zero slope in the floppy region as there are no restoring forces. In such simulations changes in connectivity are brought about by cutting bonds between C atoms with no change in bonding type. In the present experiments, however, changes in connectivity are brought about by chemical alloying, i.e., introducing fourfold coordinated Si atoms for twofold coordinated Se atoms. Such alloying also produces growth of the chemically more stable Si-Se bonds at the expense of Se-Se bonds. The small slope $d\nu_{cs}(x)/dx$ in the floppy region is of chemical origin and results from presence of the more stable heteropolar bonds in the network at the expenses of homopolar ones with increased connectivity.

At $x \geqslant 0.20$, the average slope $d\nu_{cs}/dx$ increases by a factor of 3. The mode scattering strength variation [Figs. 13(b) and 15(b)] reveals that near $x=0.20$, CS units cross-linking chains of Se increase sharply with x. Furthermore, near $x=0.20$, the scattering strength of the minority CM (dimer and trimer links between ES and CS units) also increases with x. These results suggest that rigidity is nucleated in small CLCR structures of the type shown in Fig. 16(b). We identify the composition $x=x_c(1)=0.20$ as representing transition 1, the onset of the stiffness transition in the present glasses corresponding to a change in slope $d\nu_{cs}/dx$. The composition $x_c(1)$ correlates well with the onset of a sharp reduction in the nonreversing heat flow in corresponding glassy liquids [see Fig. 4(b)]. As the glass composition increases to $x=0.20$, network stress reduces because the network becomes mechanically critical [Eq. (1)]. The underlying enthalpic changes associated with different molecular configurations accessible to the network as the glass melts acquire a minimum. These considerations are responsible for the broad minimum in ΔH_{nr} in the $0.20<x<0.26$ composition range.

2. Rigid region

We identify the rigid region in the present glasses at $x > x_c(2) = 0.270$, where the elastic response of ES units and

CS units displays a superlinear variation on mean coordination number. In Fig. 17(b), we note that both the majority and minority ES-mode frequencies, $\nu_{es}(x)$, display a power-law behavior for the underlying local elasticity at $x>0.27$. We have deduced this power law the usual way by plotting $\log_{10}(\nu_{ES}^2-\nu_c^2)$ against $\log_{10}[\overline{r}-\overline{r}_c(2)]$, and obtain $p(\mathrm{ES}^{\mathrm{low}})=1.33(10)$ and $p(\mathrm{ES}^{\mathrm{high}})=1.43(10)$ for the majority and minority modes (Fig. 19), respectively. In this composition region, the ES modes are signatures of rigid regions of the network which consist of CLCC and CLCR structures eluded to earlier. In such structures, dimeric and trimeric ES chains are cross linked by CS units or CS chains as illustrated in Figs. 16(b) and 16(c).

It is comforting indeed to see that several numerical simulations[31,32] of elasticity in networks constrained by α and β forces reveal a power law $p=1.5$ or 1.4 for the variation of the elastic constants in harmony with the present results. These numerical results suggest that the composition $x=x_c(2)=0.27$ thus marks the completion of the stiffness transition that was initiated at $x=x_c(1)=0.20$, and label $x_c(2)$ as transition 2.

We now comment on the observed $\nu_{cs}(x)$ variation at $x>x_c(2)$. In general, CS tetrahedra occur in three structural entities in the present glasses. Such tetrahedra cross link (a) Se_n chains, (b) out-of-phase ES chains in the CLCR structure, and (c) in-phase ES chains in CLCC structure. Thus while units in (a) represent the floppy part of the network, units in (b) and (c) represent the rigid part of the network. Since the concentrations of these units (a), (b), and (c) changes systematically with *x*, the underlying local elasticity $\nu_{cs}^2(x)$ variation reveals subtle changes. For example, we observe a dual power law [Fig. 19(a)], a lower power $p_r=1.15(10)$ near $x=x_c(2)$, but a higher power at $x>0.29$ of $p_{r'}=1.62(10)$. At $x>0.29$, contributions to the local elasticity due to the floppy Se_n segment decrease remarkably (Fig. 12) and the optical elasticity measurements sample the rigid phase of the network yielding the anticipated higher power law.

3. Transition region

In the transition region, i.e., $x_c(1)<x<x_c(2)$ between the *onset* and *completion* of rigidity, the present results on $\mathrm{Si}_x\mathrm{Se}_{1-x}$ glasses reveal that the local elasticity varies *sublinearly* with a reduced power law, $p_t=0.71(10)$. The power law p_t was obtained by plotting $\log_{10}[\nu_{cs}^2(x)-\nu_c^2(1)]$ against $\log_{10}[\overline{r}-\overline{r}_c(1)]$ in Fig. 18. The present Raman results also reveal that as viewed by CS mode frequency variation, transition 1 is clearly second order in $\overline{r}$. On the other hand, ES-mode frequency variations, both for majority and minority modes [Fig. 14(a)], reveal that transition 2 is first order in nature because of a small but sudden jump in mode frequency near $x=0.27$. This is a delicate result and is localized on the rigid regions comprising the CLCC and CLCR structures. In a generic sense this result is reminiscent of the intrinsically heterogeneous character of a glass on a molecular scale and the power of Raman scattering to probe the rigid and the floppy regions *independently*.

There are two other observations on these glasses that are directly correlated with our Raman stiffness results. First, the nonreversing heat flow, $\Delta H_{nr}(x)$, deduced from our MDSC

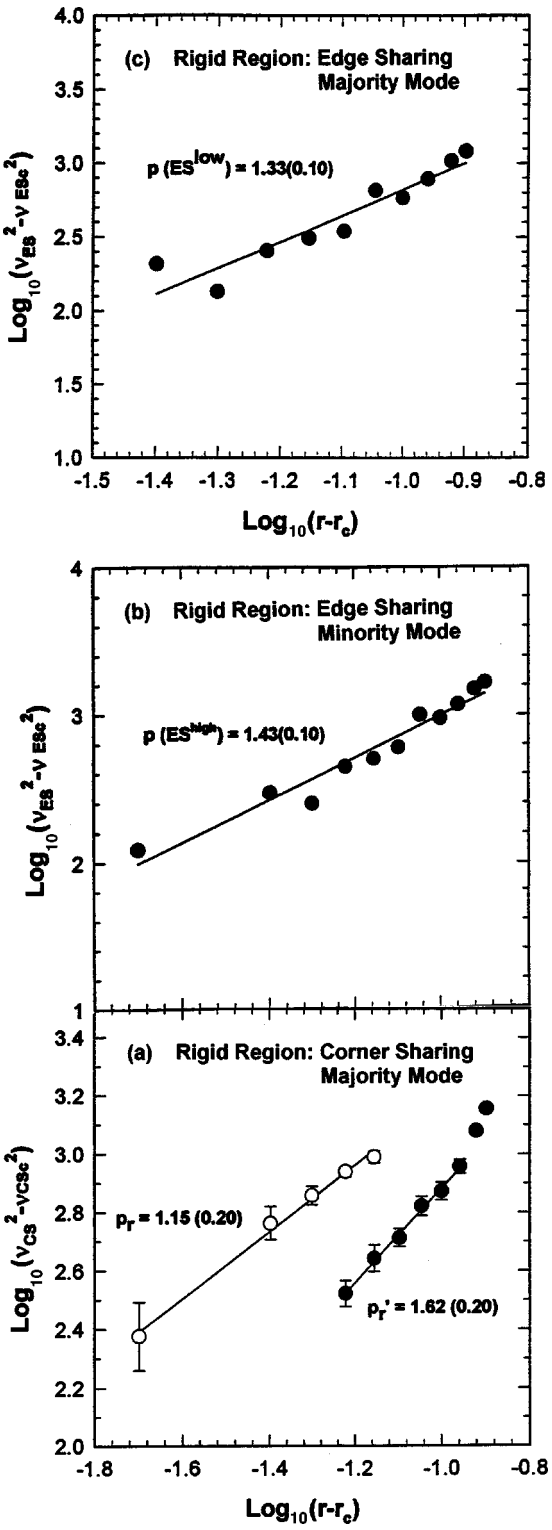

FIG. 19. Local elasticity in the rigid region starts out (a) with a power law $p_r=1.15(10)$ and acquires a power law $p_r'=1.62(10)$ at $x>0.29$ for corner sharing mode. Parallel results for the majority ES mode (b) show a power law $p(\mathrm{ES}^{\mathrm{low}})=1.33(10)$ for the majority mode and (c) a power law $p(\mathrm{ES}^{\mathrm{high}})=1.43(10)$ for the minority mode.

measurements, shows a deep and flat minimum in the transition region. In this composition range, the rigid (CLCC and CLCR structures) and floppy (Se_n chains) fragments of the backbone are finely dispersed. This results in a minimum of

network stress and minimal entropic changes when the glass softens upon heating to T_g resulting in the broad minimum in $\Delta H_{nr}(x)$. These trends mimic the activation energies for stress relaxation $E_A(\overline{r})$ in chalcogenide glasses reported by Böhmer and Angell.[33] These observations conform to the Phillips glass condition [Eq. (1)] which expresses a mechanical critical point of the system. Specifically, these observations suggest that networks in the transition region occupy the lowest (global) minimum of the energy hypersurface and that energy barriers between local minima get smaller as one approaches the global minimum of the energy hypersurface. The concept of an energy hypersurface has been invoked[34] to describe the nonergodic behavior of glass formation from melts. The second correlation occurs with molar volumes of these glasses reported by Johnson *et al.*[29] that show a broad minimum in the transition region. These results taken together reveal that in the transition region, fine dispersions of floppy and rigid regions coexist not only minimizing network strain but also leading to the most compact packing. In the transition region the glass structure evolves in a reversible fashion always trapped in the lowest energy state of the energy hypersurface ($\Delta H_{nr} \rightarrow 0$).

In general, in percolation models of rigidity, elasticity power law $p > 1.4$ are expected. To obtain a value $p < 1$, one must invoke large scale (or long-range) fluctuations such as are discussed[35] in equilibrium-scaling theory. Because ΔH_{nr} is so small in the transition region, it is reasonable to compare our fitted value of $p_t = 0.71(10)$ with the smallest value obtainable by finite-size scaling,[35] which is $2/d = \frac{2}{3}$. The value $p_t = 0.71(10)$ is much below 1.4 to be understood in terms of short-range percolation models. These ideas are consistent with the notion that in the transition region the backbone consists not only of rigid and floppy fragments that are strain free ($\Delta H_{nr} \rightarrow 0$) but also have a long coherence length ($p < 1$).

As a final comment in this section, it would be pertinent to mention that optical elastic constants (ν^2) in glasses obtained from the present Raman-scattering measurements provide a local elastic response of the backbone. These results permit one to establish which of the building blocks (CS, ES, or Se chains) forms part of the percolatively rigid backbone as the connectivity increases above a threshold. Such results are to be contrasted to bulk elastic constants on glasses deduced from ultrasonic echoes or Brillouin scattering. The latter involve long-wavelength excitations and provide elastic constants that are a global average over the glass. And for that reason not surprisingly where results are available[6] (Ge-Se glasses) bulk elastic constants are found to be structureless. We are not aware of bulk elastic constant results on the Si-Se binary.

D. Stiffness transition in Si_xSe_{1-x} and Ge_xSe_{1-x} glasses compared

There is a parallel in the stiffness transitions between the present binary system and a companion IV-VI system, the Ge_xSe_{1-x} binary. Examination of Raman scattering in the transition region, $0.20 < x < 0.24$ also reveals two transitions;[6] the *onset* of the stiffness transition (transition 1) occurs near $x = x_c(1) = 0.20$ or $\overline{r_c}(1) = 2.40$ and a completion of the transition (transition 2) at $x = x_c(2) = 0.2275$ or $\overline{r_c}(2) = 2.46$. In the Ge_xSe_{1-x} binary both transitions 1 and 2 appear to be second order in character as viewed by the CS mode frequency variation. Thus transition 1, in both binary glass systems, occurs near $\overline{r_c}(1) = 2.40$ close to the predicted mean-field value. Transition 2, on the other hand, appears to be upshifted in $\langle r \rangle$ by differing amounts in the two glass systems. It is quite likely that these differences stem from the underlying molecular structures of the glasses and these ideas will be developed in forthcoming publications.

Recent numerical simulations[36] on organized networks have shown two rigidity transitions, one at $r_c(1) = 2.375$ from a floppy to an unstressed rigid phase, and a second one at $r_c(2) = 2.392$ from an unstressed rigid to a stressed rigid phase. Although the numerically predicted elastic thresholds $(r_c(1), r_c(2))$ are lower than the experimental ones $(r_c(1) = 2.40,\ r_c(2) = 2.54)$, nevertheless, the numerical results provide insights. The simulations show that real glasses near the rigidity transitions are organized at some level and not random networks, and that the intermediate phase $[r_c(1) < r < r_c(2)]$ may be characterized by a stress-free backbone. And it is possible that the thermally reversing character of glass transition in the intermediate phase is a manifestation of the stress-free nature of the backbone.

V. CONCLUSIONS

Raman-scattering measurements on Si_xSe_{1-x} glasses in the Se-rich compositions, $0 < x < \frac{1}{3}$, reveal modes of CS and ES $Si(Se_{1/2})_4$ tetrahedra and of Se_n chain modes which are symmetric Gaussians at low x ($x < 0.19$). At higher x, the line shape of these modes becomes asymmetric, and each of these modes requires at least two Gaussians for a deconvolution. Global variation of mode parameters such as frequency, scattering strength, and linewidth as a function of Si concentration suggest a change in molecular structure from a Se_n chain network randomly cross linked by ES and CS tetrahedra at low x, to a network largely consisting of ES chains cross linked by CS tetrahedra, as $x \rightarrow \frac{1}{3}$. Mode frequency variation of the majority CS mode provides evidence of two transitions in local elasticity; transition 1 at $x = x_c(1) = 0.20$ or $\overline{r_c}(1) = 2.40$ marking the onset of rigidity and transition 2 at $x = x_c(2) = 0.265$ or $\overline{r_c}(2) = 2.53$ marking the completion of rigidity. These results correlate well with the nonreversing heat flow $\Delta H_{nr}(x)$ measurements deduced from temperature modulated DSC which reveal a broad minimum in the transition region $x_c(1) < x < x_c(2)$ and a progressively increasing value of ΔH_{nr} as the network gets either floppy $x < x_c(1)$ or rigid $x > x_c(2)$.

ACKNOWLEDGMENTS

We acknowledge with pleasure discussions with B. Goodman, M. F. Thorpe, and J. C. Phillips during the course of this work. This work was supported by NSF Grant Nos. DMR-97-02189 and DMR-94-24556.

[1] W. J. Bresser, P. Boolchand, and P. Suranyi, Phys. Rev. Lett. **56**, 2493 (1986).
[2] J. C. Phillips, J. Non-Cryst. Solids **34**, 153 (1979); **43**, 37 (1981).
[3] M. F. Thorpe, J. Non-Cryst. Solids **57**, 355 (1983).
[4] X. Feng, W. J. Bresser, M. Zhang, B. Goodman, and P. Boolchand, J. Non-Cryst. Solids **222**, 137 (1997).
[5] M. F. Thorpe in *Insulating and Semiconducting Glasses*, edited by P. Boolchand (World Scientific, Singapore, 2000), p. 95.
[6] X. Feng, W. J. Bresser, and P. Boolchand, Phys. Rev. Lett. **78**, 4422 (1997); P. Boolchand, X. Feng, D. Selvanathan, and W. J. Bresser, *Rigidity Theory and Applications*, edited by M. F. Thorpe and P. M. Duxbury (Plenum, New York, 1999), p. 279.
[7] A. N. Sreeram, A. K. Varshneya, and D. R. Swiler, J. Non-Cryst. Solids **128**, 294 (1991).
[8] S. Mahadevan, A. Giridhar, and A. K. Singh, J. Non-Cryst. Solids **57**, 423 (1983).
[9] W. A. Kamitakahara, R. L. Cappelletti, P. Boolchand, B. Halfpap, F. Gompf, D. A. Neumann, and H. Mutka, Phys. Rev. B **44**, 94 (1991).
[10] P. Boolchand, W. Bresser, M. Zhang, Y. Wu, J. Wells, and R. Enzweiler, J. Non-Cryst. Solids **182**, 143 (1995).
[11] J. C. Phillips, in *Rigidity Theory and Applications*, edited by M. F. Thorpe and P. Duxbury (Plenum, New York, 1999), p. 155.
[12] R. W. Johnson, D. L. Price, S. Sussman, M. Arai, T. I. Morrison, and G. K. Shenoy, J. Non-Cryst. Solids **83**, 251 (1986).
[13] M. Tenhover, M. A. Hazle, and R. K. Grasselli, Phys. Rev. Lett. **51**, 404 (1983).
[14] J. E. Griffiths, M. Malyj, G. P. Espinosa, and J. P. Remeika, Phys. Rev. B **30**, 6978 (1984).
[15] S. Susman, R. W. Johnson, D. L. Price, and K. J. Volin, in *Defects in Glasses*, edited by F. L. Galeener, D. L. Griscom, and M. J. Weber, MRS Symposia Proceedings No. 61 (Materials Research Society, Pittsburgh, 1986), p. 91.
[16] S. Sugai, Phys. Rev. B **35**, 1345 (1987).
[17] M. Tenhover, R. S. Henderson, M. A. Hazle, D. Lukco, and R. K. Grasselli, in *Design of New Materials*, edited by D. L. Cocke and A. Clearfield (Plenum, New York, 1987), p. 329.
[18] M. Tenhover, R. D. Boyer, R. S. Henderson, T. E. Hammond, and G. A. Shreve, Solid State Commun. **65**, 1517 (1988).
[19] R. W. Johnson, S. Susman, J. McMillan, and K. J. Volin, Mater. Res. Bull. **21**, 41 (1986).
[20] B. Wunderlich, Y. Jin, and A. Boller, Thermochim. Acta **238**, 277 (1994).
[21] D. Selvanathan, Masters thesis, University of Cincinnati, 1998.
[22] A. Weiss and A. Weiss, Z. Naturforsch. B **7**, 483 (1952); also see Z. Anorg. Allg. Chem. **276**, 95 (1954).
[23] V. Michel-Lledos, Ph.D. thesis, University of Montpellier II, 1991.
[24] A. Pradel, V. Michel-Lledos, M. Ribes, and H. Eckert, Chem. Mater. **5**, 377 (1993).
[25] G. Dittmar and H. Schäfer, Acta Crystallogr., Sect. B: Struct. Crystallogr. Cryst. Chem. **B32**, 2726 (1976).
[26] L. F. Gladden and S. R. Elliott, J. Non-Cryst. Solids **109**, 211 (1989); **109**, 223 (1989).
[27] R. Zallen and G. Lucovsky, in *Selenium*, edited by R. A. Zingaro and W. C. Cooper (Van Nostrand Reinhold, New York, 1974).
[28] M. H. Brodsky, R. J. Gambino, J. E. Smith, and Y. Yacoby, Phys. Status Solidi B **52**, 609 (1972).
[29] R. Kerner and M. Micoulaut, J. Non-Cryst. Solids **210**, 298 (1997).
[30] D. A. Drabold, in *Insulating and Semiconducting Glasses*, edited by P. Boolchand (World Scientific, Singapore, in press); P. Vashishta, R. K. Kalia, A. Nakano, W. Li, and I. Ebbsjo, in *Amorphous Insulators and Semiconductors*, edited by M. F. Thorpe and M. I. Mitkova (Kluwer Academic, London, 1996), p. 151.
[31] H. He and M. F. Thorpe, Phys. Rev. Lett. **54**, 2107 (1985).
[32] D. S. Franzblau and J. Tersoff, Phys. Rev. Lett. **68**, 2172 (1992).
[33] R. Böhmer and C. A. Angell, Phys. Rev. B **45**, 10091 (1992).
[34] H. Fraunfelder, A. R. Bishop, A. Garcia, A. Perelson, P. Schuster, D. Sherington, and P. J. Swart, Physica D **107**, 117 (1997).
[35] J. C. Phillips (private communication); B. D. Josephson, Phys. Lett. **21**, 608 (1966); J. T. Chayes, L. Chayes, D. S. Fisher, and T. Spencer, Phys. Rev. Lett. **57**, 2999 (1986).
[36] M. F. Thorpe, D. J. Jacobs, M. V. Chubynsky, and J. C. Phillips (unpublished).